Human Pathology (2019) **86**, 203–212

ELSEVIER

Human PATHOLOGY

www.elsevier.com/locate/humpath

Original contribution

Clinicopathological and molecular analysis of multinodular and vacuolating neuronal tumors of the cerebrum☆,☆☆,★

Euno Choi MD[a,1], Seonk-Ik Kim MD[a,1], Jae-Kyung Won MD, PhD[a], Chun Kee Chung MD, PhD[b], Seung Ki Kim MD, PhD[b], Seung-Hong Choi MD, PhD[c], Seongmin Choi BS[d], Bome Han BS[e], Bokyung Ahn MD[f], Sun-Wha Im MD, PhD[g], Sung-Hye Park MD, PhD[a,h,*]

[a]*Department of Pathology, Seoul National University Hospital and Seoul National University College of Medicine, Seoul 03080, Republic of Korea*
[b]*Department of Neurosurgery, Seoul National University Hospital and Seoul National University College of Medicine, Seoul 03080, Republic of Korea*
[c]*Department of Radiology, Seoul National University Hospital and Seoul National University College of Medicine, Seoul 03080, Republic of Korea*
[d]*Division of Clinical Bioinformatics, Biomedical Research Institute, Seoul National University Hospital, Seoul 03080, Republic of Korea*
[e]*Department of Bioinformatics, Seoul National University Hospital and Seoul National University College of Medicine, Seoul 03080, Republic of Korea*
[f]*Department of Pathology, Korea University Hospital, College of Medicine, Seoul 02842, Republic of Korea*
[g]*Department of Biochemistry, Seoul National University Hospital and Seoul National University College of Medicine, Seoul 03080, Republic of Korea*
[h]*Institute of Neuroscience, Seoul National University College of Medicine, Seoul 03080, Republic of Korea*

Received 31 July 2018; revised 23 November 2018; accepted 30 November 2018

Keywords:
Neuronal tumors;
Epilepsy;
Ganglioglioma;
Brain;
FGFR2-ZMYND11 fusion

Summary Multinodular and vacuolating neuronal tumor (MVNT) of the cerebrum is a recently recognized rare neuronal tumor, and its pathogenesis is unclear. We analyzed 7 cases of histologically typical MVNT: 6 were adults (mean age, 43.0 years [range, 23-56 years]) and 1 was a child (age, 10 years). The most common symptoms were seizures (n = 4) and headache (n = 2). The tumors were supratentorial (temporal, 5; frontal lobes, 2) in origin as reported. Vacuolated tumor cells were robustly positive for α-INA and Olig2 and at least partly positive for synaptophysin and MAP2, but negative for Neu-N, nestin and CD34. GFAP and vimentin were expressed in reactive astrocytes but not in tumor cells. Negative results were obtained for p53, IDH-1, $BRAF^{V600E}$, H3 K27M, EGFR, Lin28A, and L1CAM. ATRX, BRG1, INI-1, and TMHH were retained.

☆ Competing interests: The authors do not have any conflict of interest to declare.
☆☆ Funding/Support: This study was supported by a grant from Korea Health Technology R&D Project through the Korea Health Industry Development Institute, funded by the Ministry of Health and Welfare, Republic of Korea (Grant No. HI14C1277) and the National Cancer Center, Republic of Korea (NCC-1810861-1).
★ Ethical publication statement: We confirm that we have read the *Journal*'s position on issues involved in ethical publication and affirm that this report is consistent with those guidelines.
* Corresponding author at: Department of Pathology, Seoul National University College of Medicine, 103 Daehak-ro, Jongno-gu, Seoul 110-799, Republic of Korea.
E-mail address: shparknp@snu.ac.kr (S. -H. Park).

https://doi.org/10.1016/j.humpath.2018.11.028

The Ki-67 labeling index was very low (<1%), and pHH3 revealed no mitotic figure. Ultrastructural features of tumor cells were comparable with those of immature neuronal cells, with several intracytoplasmic myelin-like autophagosomes and pericellular vacuolization. No *IDH1*/*IDH2* and $BRAF^{V600E}$ mutations were found upon direct sequencing. Whole-exome sequencing revealed *FGFR2-ZMYND11* gene fusion in 1 case. After gross total resection, all patients were alive without seizures. There was no tumor recurrence during an average period of 68 months (range, 23-101 months). The analysis of 7 typical cases of MVNT suggested that these lesions may be clonal tumors because *FGFR2-ZMYND11* fusion was found (1 case).

1. Introduction

Multinodular and vacuolating neuronal tumors (MVNTs) of the cerebrum have recently been reported as unusual neuronal tumors [1,2]. To date, a total of 62 cases, including cases where histopathology is not proven, have been reported. Ratilal et al [3] first reported a case with the title "diffuse cerebral gangliocytoma," which occurred in a 43-year-old man with late onset of seizures. Although some authors insisted that this entity may be a mixed neuronal and glial lesion [4,5], they are generally considered purely neuronal tumors occurring in cerebral hemispheres, predominantly affecting the temporal lobe of adults [1]. Seizures or seizure equivalents and headache are the most common clinical manifestations [1]. Histopathologically, they are characterized by multiple discrete and coalescent nodules composed of ambiguous neuron-like cells with vacuoles [1-3,6-8]. The tumor cells exhibit consistent immunolabeling for HuC/HuD, which are neuronal markers associated with earlier stages of neuronal development. Recently, genetic alterations that activate the MAP kinase signaling pathway have been reported, such as mutations in *BRAF* and exon 2 of the *MAP2K1* gene [5]. Furthermore, 1 case demonstrated an *FGFR2-INA* in-frame gene fusion.

Because it is still not clear whether multinodular and vacuolating neuronal tumor is a neoplasm or malformation, we investigated the clinicopathological characteristics of this lesion with its genetic background. Herein, we have analyzed 7 cases with typical histopathology of MVNT and evaluated clinical features and immunohistochemical findings using selected antibodies, such as Neu-N, α-INA, Olig2, synaptophysin, microtubule-associated protein 2 (MAP2), nestin, CD34, GFAP, vimentin, p53, IDH-1, BRAF VE1, H3 K27M, EGFR, Lin28A, L1CAM, ATRX, BRG1, INI-1, trimethyl histone H3 (TMHH3), MIB-1, and pHH3. Whole-exome sequencing (WES) was carried out in 4 cases. We describe an additional case with a new genetic finding.

2. Materials and methods

2.1. Cases

We retrospectively reviewed 80 cases with original pathological diagnosis of ganglioglioma (GG; n = 78), gangliocytoma (n = 1), and focal cortical dysplasia, type unclassifiable with vacuolating neuron-like cells (n = 1) by 2 pathologists (S. H. P;. and S. I. K.), from 2005 to 2016, from the pathology archives of the Seoul National University Hospital. Of these, 7 cases were considered to have typical histologic features of MVNT; however, they were previously diagnosed as GG (n = 5), gangliocytoma (n = 1), and focal cortical dysplasia, type unclassifiable with vacuolating neuron-like cells (n = 1), because they were not elsewhere classified in the World Health Organization (WHO) classification of central nervous system tumors.

2.2. Immunohistochemistry

Immunohistochemical staining was performed using the most representative formalin-fixed, paraffin-embedded (FFPE) tissues of 3-μm thickness using an automated immunostainer (Ventana BenchMark XT, Tucson, AZ) according to the manufacturer's protocol. Primary antibodies used were as follows: NeuN, α-INA, Olig2, synaptophysin, MAP2, nestin, CD34, GFAP, vimentin, p53, IDH-1, BRAF VE1, H3 K27M, EGFR, Lin28A, L1CAM, ATRX, BRG1, INI-1, TMHH3, MIB-1, and pHH3 (Supplementary Table 1).

2.3. Electron microscopy

Electron microscopic examination was carried out on fresh tumor tissues in 4 cases. Tissues were fixed in a cold 2.5% glutaraldehyde solution. Tissues were postfixed for 1.5 hours in 2% osmium tetroxide and in 0.1 M phosphate buffer for 1.5 hours at room temperature. Samples were then washed briefly with 0.1 M phosphate buffer, dehydrated through a graded 50-60-70-80-90-95 and 100% ethanol series, and finally embedded in epoxy resin. Appropriate areas for thin sectioning were cut at 65 nm and stained with saturated 4% uranyl acetate and 4% lead citrate before examination with a transmission electron microscope (JEM-1400; JEOL, Akishima, Japan) at 80 Kv.

2.4. DNA extraction

Genomic DNA was extracted from FFPE tissues of 4 cases using Promega (Madison, WI) DNA extraction kits, which were validated using Nanodrop and PicoGreen. All the samples passed the quality threshold for Sanger sequencing and next-generation sequencing.

Table 1 Clinical findings of our 7 cases

Case	Sex	Age (y)	Clinical manifestation (duration of symptoms)	Lesional location	Operation	Follow-up (y)	Postoperative medication (seizure status)	Recurrence
1	M	10	Seizure (for 1 mo)	Lt temporal	GTR	8.4	Levetiracetam 250 mg BID (seizure-free)	No
2	M	51	Headache (for 3 mo)	Rt temporal	GTR	8.2	No (symptom-free)	No
3	M	56	Headache (for 1 y)	Rt frontal (cingulate)	GTR	5.7	No (seizure-free; occasional headache)	No
4	M	23	Seizure (age, 3-15 y) and headache (for 2 y)[a]	Rt frontal	GTR	4.9	No (symptom-free)	No
5	F	37	Seizure (16 y)	Rt temporal	GTR	5.3	Phenytoin 100 mg BID (seizure-free)	No
6	M	42	Incidental finding (Meniere disease)	Rt temporal (uncus)	GTR	2.1	No (symptom-free)	No
7	M	49	Seizure (for 10 y)	Lt temporal	GTR	1.9	Valproic acid 500 mg BID (seizure-free)	No

Abbreviations: BID, twice a day; F, female; GTR, gross total removal; Lt, left; M, male; Rt, right.

[a] Patient 4 had a history of intractable epilepsy for 13 years (as a 3-year-old to 15-year-old) and thereafter, seizures were controlled by antiepileptic drugs, but intermittent headache developed for 2 years before surgical intervention.

2.5. Genomic sequencing

Sanger sequencing analyses for *IDH1*, *IDH2*, and $BRAF^{V600E}$ were performed on an the ABI DNA sequencing platform (Applied Biosystems 3500 series; Thermo Fisher Scientific, Waltham, MA) using primer sets and polymerase chain reaction (PCR) methods that we described previously [9,10].

2.6. Whole-exome sequencing

With genomic DNA extracted from 4 cases (cases 4-7) of FFPE tumor tissues by gross macrodissection, WES was performed using a HiSeq2500 instrument (Illumina, San Diego, CA) and 101-bp paired-end reads.

For the generation of standard exome capture libraries, we used the Agilent (Santa Clara, CA) SureSelect Target Enrichment protocol for Illumina paired-end sequencing library (ver. B.3, June 2015) together with 1 μg input gDNA. In all cases, the SureSelect Human All Exon V6 probe set was used.

Fragmentation of 1 μg of genomic DNA was performed using adaptive focused acoustic technology (Covaris, Woburn, MA). The fragmented DNA was repaired, an "adenosine nucleotide" was ligated to the 3′ end, and Agilent adapters were then ligated to the fragments. Once ligation had been assessed, the adapter-ligated product was PCR amplified. The final purified product was then quantified using qPCR according to the qPCR Quantification Protocol Guide and qualified using the TapeStation DNA screentape D1000 (Agilent). For exome capture, 250 ng of DNA library was mixed with hybridization buffers, blocking mixers, RNase block, and 5 μL of SureSelect all exon capture library, according to the standard Agilent SureSelect Target Enrichment protocol. Hybridization to the capture baits was conducted at 65°C using the heated lid option at 105°C for 24 hours on the thermal cycler.

The captured DNA was then amplified. The final purified product was quantified using qPCR according to the qPCR Quantification Protocol Guide and qualified using the TapeStation DNA screentape D1000 (Agilent). We then sequenced the amplification product using the NovaSeq platform (Illumina). The result of WES is described in Supplementary Table 2.

We used default option of Control-FREEC (6.4) for copy number variant (CNV). We created a configuration file, such

Table 2 MRI findings of our 7 cases

Case	Site	Circumscription	Cyst	T2	T1	Enhancement	Satellite nodules	Size (cm)
1	Lt temporal	Ill-defined	(+)	High	Low	(−)	(−)	1.7 × 1.2
2	Rt temporal	Ill-defined	(−)	High	Slightly low	(−)	(−)	3.7 × 2.1
3	Rt frontal (cingulate)	Ill-defined	(−)	High	Iso or low	(−)	(−)	1.6 × 1.6
4	Rt frontal	Well-defined	(−)	High	Iso	(−)	(−)	1.9 × 1.2
5	Rt temporal	Well-defined	(+)	High	Iso or low	Partial	(−)	2.3 × 2.0
6	Rt temporal (uncus)	Ill-defined	(−)	High	ND	(−)	(−)	2.8 × 2.0
7	Lt temporal	Ill-defined	(+)	High	Iso or low	(−)	(+)	3.5 × 2.4

Abbreviations: High/Iso/Low, high/iso/low signal intensity; Lt, left; ND, no data; ;Rt, right; +, present; −, absent.

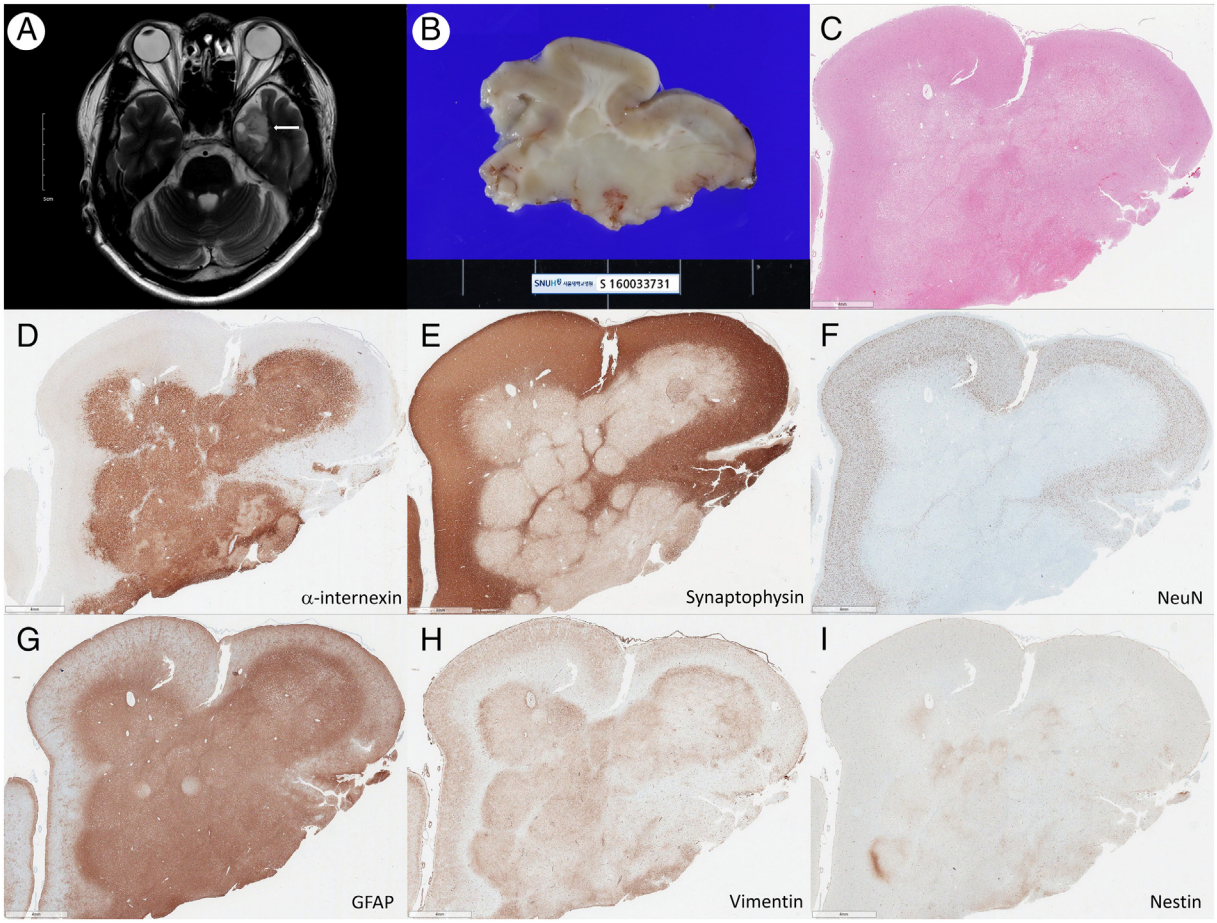

Fig. 1 Magnetic resonance image, gross, histologic, and immunohistochemical findings of case 7 (male/49 years old). A, Relatively well-demarcated T2 high-signal intensity tumor with peripheral lobulation present in the left temporal lobe. B, The typical multinodular feature of the tumor is well revealed grossly. C, Light microscopic image also shows vague multinodularity. On immunohistochemistry, the tumor was observed to be well delineated by α-internexin (D) and vimentin (H). E, Synaptophysin was weakly positive in the tumor. F, Neu-N was negative in tumor cells and in the background of the tumor. GFAP was strongly positive in the background of the tumor (G), whereas nestin was only focal weakly positive in the background of the tumor (I). A, T2-weighted image; B, gross; C, hematoxylin and eosinE, ;; D-I, α-INA, synaptophysin, Neu-N, GFAP, vimentin, and nestin; C-I, original magnification x1.

that the window size of the general record was set as 500 and bam files were set for each sample. Result analysis of CNV type is classified based on genome ploidy value 2; values below 2 indicate loss and those above 2 indicate gain. Visualization of CNV was conducted using R 3.2.1 (www.r-project.org). Added CNVs were identified using the CNVkit (0.8.1) with a default option for single sample. CNVkit is a software used to infer and visualize from targeted DNA sequencing data (https://cnvkit.readthedocs.io/en/v0.8.1/pipeline.html).

3. Results

3.1. Clinical and radiologic findings

Patients' clinical findings are summarized in Table 1. The male-to-female ratio was 6:1, and the mean age of adult patients was 43 years (range, 23-56 years). A 10-year-old boy was also included. The order of typical symptoms was seizure (n = 4) and headache (n = 2), whereas 1 case (case 6) was found incidentally during workup for Meniere disease. The duration of seizures was 1 month (child case) and 10 to 16 years (adult cases). All 7 cases involved the cerebral hemispheres ;: the temporal (n = 5) and frontal lobes (n = 2).

On the magnetic resonance imaging (MRI), the tumors were found as solid multilobulated lesions, and 3 cases (43%) showed focal cystic changes (Table 2). Epicenter of the tumors was the subcortical white matter with involvement of the junction of the gray-white matter. All tumors were hyperintense in T2-weighted or FLAIR images and isointense or hypointense in T1-weighted image (Supplementary Fig. 1). Generally, tumors were not well demarcated on T2-weighted images, but 2 cases (cases 4 and 5) were relatively well demarcated. Mostly, there was no enhancement or mass effect, but 1 case (case 5) showed partial enhancement and minimal perilesional

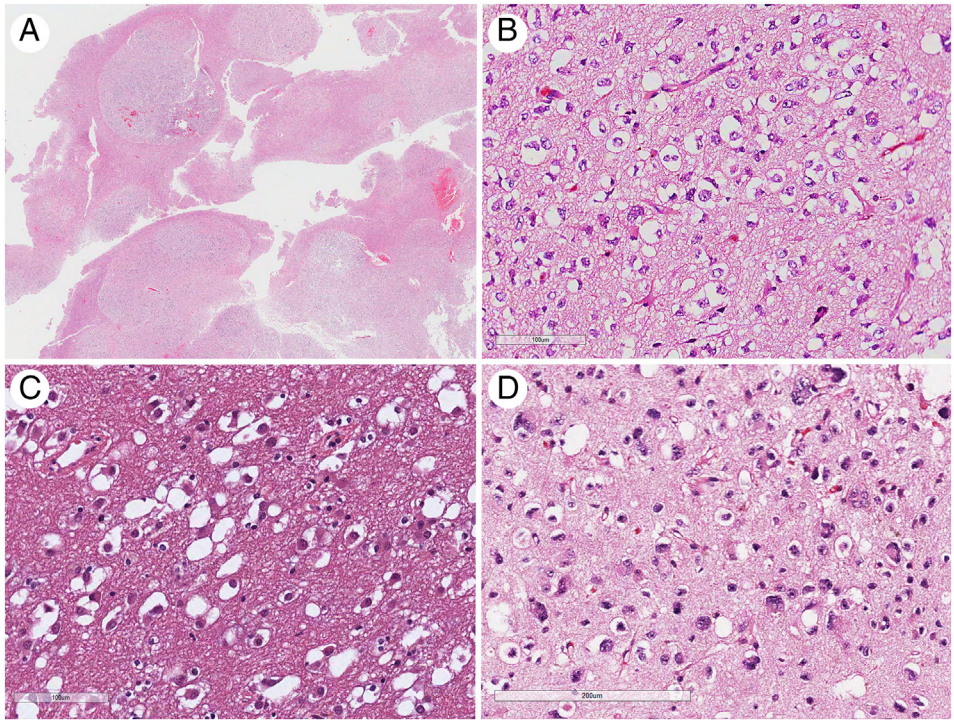

Fig. 2 Representing histologic findings. A, Low-power view of case 4 shows multiple discrete nodules. B, Tumor cells show ambiguous neuron-like appearance having 1 or 2 vesicular nuclei and cytoplasmic and pericellular variously-shaped vacuoles. C, Pericellular eccentric vacuoles are prominent in case 1. D, Some of the nodules show pleomorphic nuclei, which might be derived from degenerative atypia caused by its slow-growing nature (case 4). In all cases, there were no other anaplastic features, such as mitoses, necrosis, or microvascular proliferation. A-D, E;Hematoxylin and eosin, original magnifications ×1 (A) and ×200 (B-D).

edema was noted in case 1 (Supplementary Fig. 1). The largest diameter of the tumor was up to 3.5 cm (range, 1.6-3.5 cm). Each radiologic finding is depicted in Table 2.

3.2. Treatment and follow-up

All patients underwent craniotomy and gross total resection of tumor. None of the patients underwent adjuvant chemotherapy or radiotherapy. The median follow-up period was 68 months (range, 23-101 months). All 4 patients with preoperative seizures were seizure-free during the follow-up period after surgery. However, 3 of them are still taking antiepileptic drugs (Table 1). There was no tumor recurrence. At the final follow-up, all patients had no symptoms, except one who had an occasional headache. The 10-year-old boy underwent a second operation 6 years after the initial surgery because of sustained seizures caused by a small residual tumor (0.5 cm in diameter; case 1).

3.3. Histopathologic features

Microscopically, tumors showed multiple discrete and coalescent nodules (Figs. 1 and 2). The tumors were located in the subcortical regions in the white matter, with or without involvement of the deep gray matter, resembling neuronal heterotopia. They were mainly composed of immature-appearing or ambiguous neuronal cells with round, vesicular nuclei having prominent nucleoli and enlarged eosinophilic or coarsely vacuolated cytoplasm, where no definite Nissl substances were noted (Fig. 2). Pericellular eccentric vacuolization was noted. Tumor cells did not exhibit overt cellular atypia except in 2 cases; case 4 showed pleomorphism and multinucleation, and case 1 demonstrated pleomorphic nuclei in the specimen obtained from a "second-look" operation. The second resected specimen proved small residual tumor. There was no mitosis at all in any tumor. There were no Rosenthal fibers, eosinophilic granular bodies, perivascular lymphocytic infiltration, or microcalcification. Moreover, there were no oligodendroglia-like cells.

3.4. Immunohistochemical findings

The most remarkable immunohistochemical finding was the robust expression of α-INA in the membrane of tumor cells and background neuropil in all cases except cases 2 and 4. α-INA was well delineated in tumor nodules (Figs. 1D and 3A). Synaptophysin was expressed in the background neuropil in nearly all tumors (Figs. 1E and 3H). The tumor cells were strikingly positive for Olig2 but negative for NeuN (Fig. 3E-G). MAP2 was expressed in part of tumor cells in all cases, which delineated tumor nodules well in some cases (Fig. 3B). CD34 and Nestin were negative in the tumor cells (Figs. 3C and 3D). CD34 expression was diffuse and

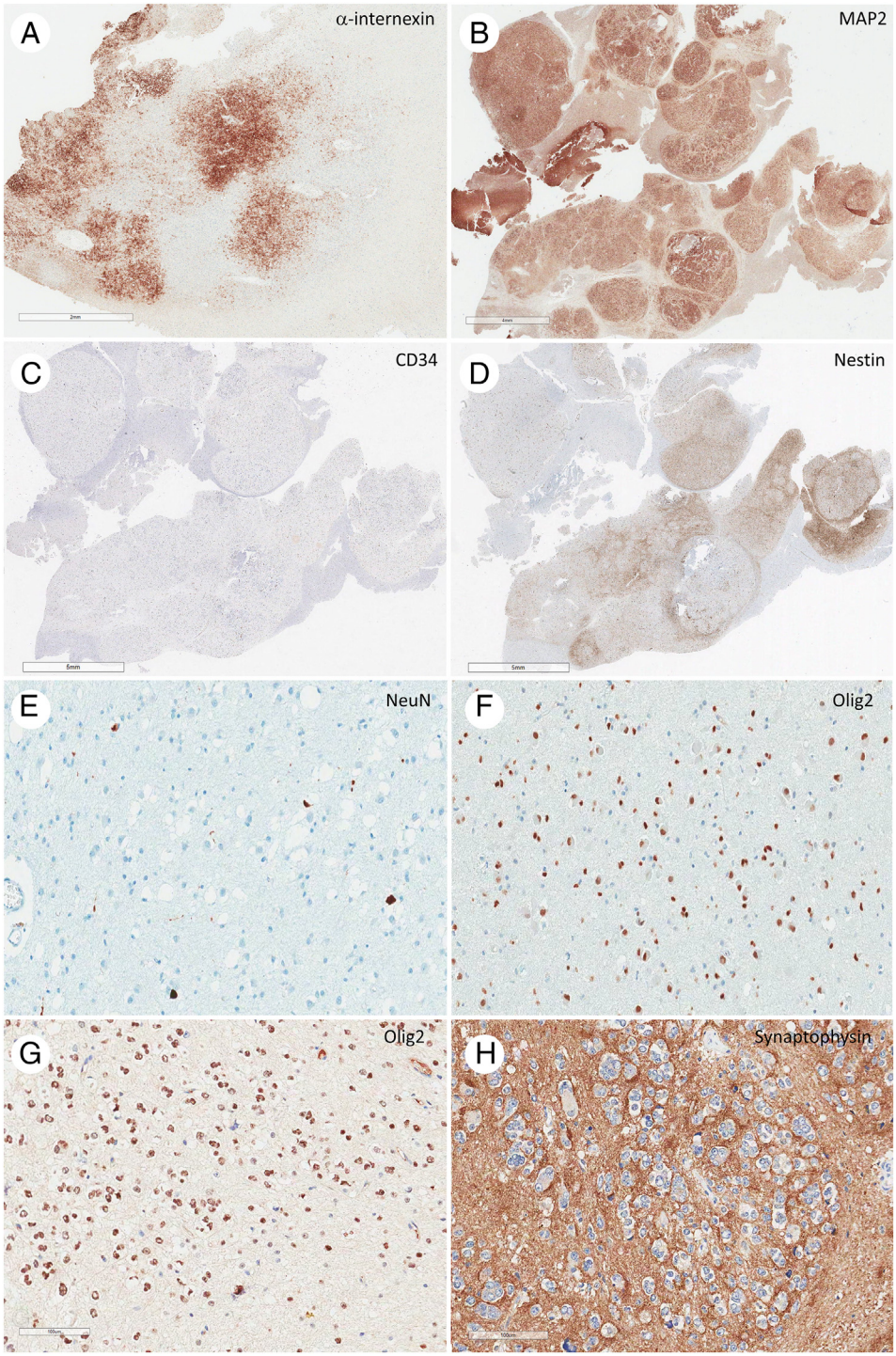

Fig. 3 Immunohistochemical staining at low and high magnifications. A, Low-power view of case 1 (10-year-old boy) showed robust positivity for α-internexin. B, MAP2 well delineates tumor nodules in case 7 (49-year-old man). C, Unlike the other cases, CD34 was negative in tumor cells. D, Nestin was also negative in the tumor cells. E, Most tumor cells were nonreactive to Neu-N. F and G, Olig2 was partly or diffusely positive in tumor cells. H, Synaptophysin was mainly positive in the background, and cytoplasm was stained with weak-to-moderate degree of intensity. Original magnifications ×1 (B-D), ×10 (A), and ×200 (E-H).

patchy in 1 case (case 1, Fig. 3C) in a ramified pattern. IDH-1, $BRAF^{V600E}$, p53, H3 K27M, EGFR, Lin28A, and L1CAM were completely negative in all cases. ATRX, BRG1, INI-1, or TMHH3 showed retained expression. GFAP expression was restricted to the background and reactive astrocytes (Fig. 1). Vimentin also highlighted reactive astrocytes but was not stained in tumor cells. Ki-67–positive tumor cells were rarely found (Ki-67 index <0.1). pHH3 revealed no mitotic figure.

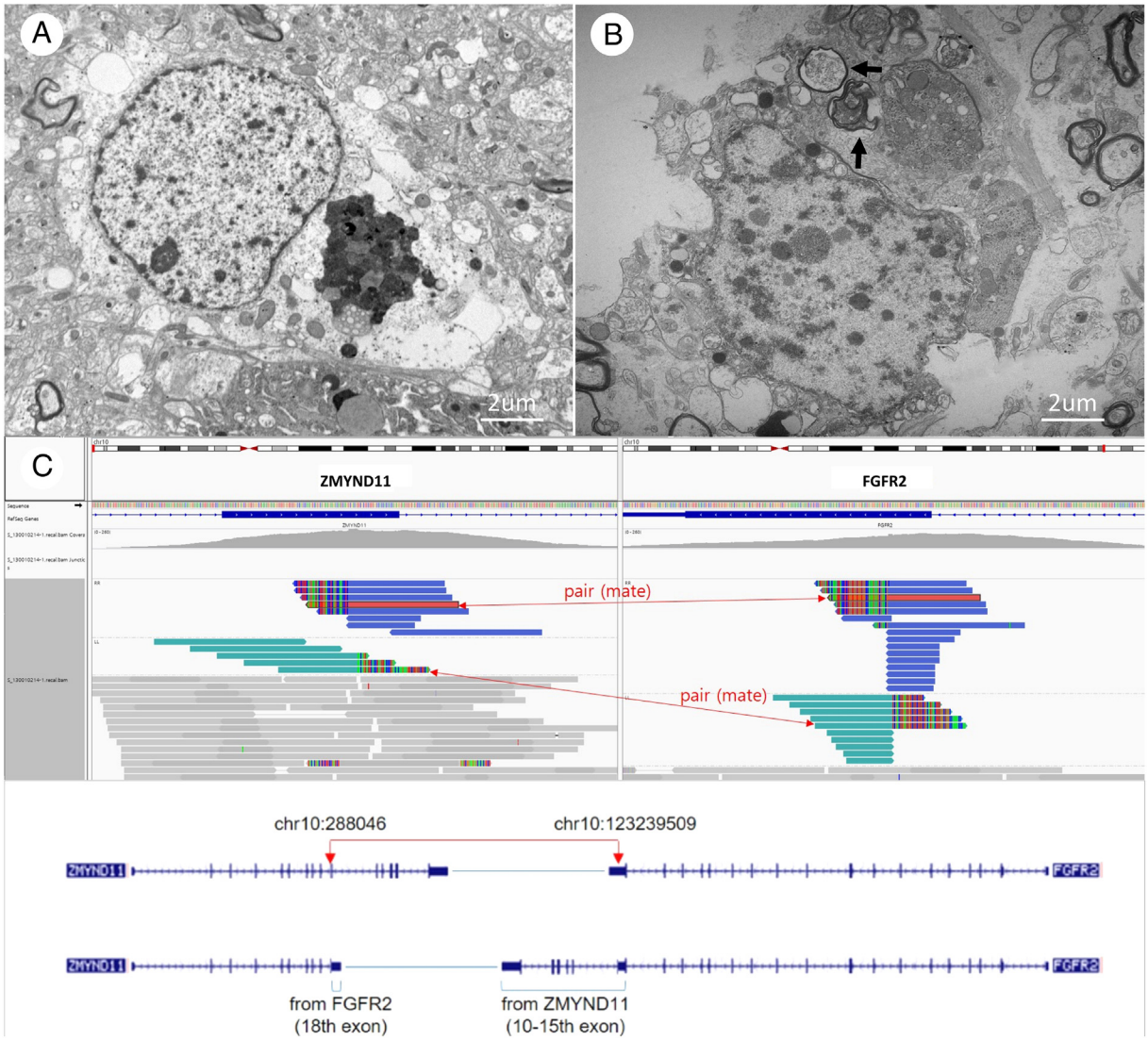

Fig. 4 Representing electron microscopic findings (A and B), snapshot from the Integrative Genomics Viewer (IGV; C), and diagram based on genetic study (D). A, The immature neuronal cells have a round nucleus, and the cytoplasm contains mitochondria and somewhat dilated RER, with large lipofuscin (enigmatic body–like) or myelin appearing in degenerated organelles (arrows). B, The nucleus shows mildly irregular contours and chromatic clumping. The cytoplasm contains myelin-figured wear-and-tear organelles (autophagolysosomes). There was empty space around the tumor cells, and the punch-out cytoplasm is present. C, IGV shows *FGFR2-ZMYND11* gene fusion on chromosome 10. Breakpoint spanning sequences revealed that orientation of read pair follows in the same direction. Because expected orientation of pair is normally facing inward, we speculated that inversion occurred. In our diagram of chromosomal inversion, the upper picture shows *ZMYND11* and *FGFR2* on normal chromosome and suspected breakpoint localization. The lower picture shows the result of inversion. Suspected breakpoint is on *ZMYND11* between position chr10: 288,046-288,047 and breakpoint on *FGFR2* between position chr10: 123,239,509 and 123,239,510. Each breakpoint is located in the 10th exon of *ZMYND11* (NM_006624.5) and 18th exon of *FGFR2* (NM_000141.4), respectively. The sequence between *ZMYND11* and *FGFR2* is drawn in a shortened form because the size of intron is too long.

3.5. Electron microscopic findings

Ultrastructurally, the vacuolated cells resembled degenerating and immature neurons. The nuclei exhibited a rounded appearance with slight peripheral clumping of chromatin and occasionally conspicuous nucleoli. The cytoplasm contained mitochondria and dilated rough endoplasmic reticulum (RER) cisternae. The characteristic feature of these cells is myelin-like or enigmatic body (lipofuscin)–like autophagolysosomes. The existing RER cisternae were not sufficient for the Nissl substances. The vacuoles that appeared around the tumor cells were actually empty spaces (Fig. 4A and B).

3.6. Direct sequencing

IDH1/*IDH2* and $BRAF^{V600E}$ mutations were not detected in any of the cases.

Table 3 Summaries of the previously reported cases including our 7 cases [1-8,11-19]

Item	No. of patients
Age (y), child/adult	6/63 (range, 6-71)
Mean age of children (y)	11.6
Mean age of adult (y)	43.4
Male-to-female ratio	32:37 (1:1.15)
Symptoms	
Seizures	32 (46.4%), du: 1 mo to >40 y
Headache	19 (27.5%), du: days to 6 y
Visual symptoms	4 (5.8%)
Paresthesia/tingling/numbness	4 (5.8%)
Dizziness	3 (4.3%)
Confusion	2 (2.9%)
Dysarthria	2 (2.9%)
Gustatory movement	1 (1.4%)
Spasm	1 (1.4%)
Staring and mumbling	1 (1.4%)
Cognitive impairment	1 (1.4%)
None	3 (4.3%)
Rt hemisphere/Lt hemisphere	35/29 (NM: 5)
Temporal	27 (41.5%)
Frontotemporal	2 (3.1%)
Parietotemporal	1 (1.5%)
Frontal	19 (29.2%)
Frontoparietal	1 (1.5%)
Parietal	9 (13.8%)
Occipital	5 (7.7%)
Parietooccipital	1 (1.5%)
NM	4 (5.8%)
MRI	
T2 high	68 (NM: 1)
T1 low and or iso	51 (NM: 17, mild high: 1)
Enhanced/nonenhanced	5/47 (NM: 17)
Satellite nodules +/−	25/23 (NM: 21)
Recurrent	0

Abbreviations: du, duration; Lt, left; NM, not mentioned; Rt, Lt: Left ; NM: Not mentioned;right.

3.7. Whole-exome sequencing

WES was carried out in 4 tumors. A total of 96, 49, 90, and 63 single-nucleotide variants and INDELs were delineated, respectively. However, there were no significant single-nucleotide variant or INDEL or copy number alterations identified by log2 ratio, B-allele frequency, and segmentation heatmap. However, 1 case revealed an *FGFR2-ZMYND11* intrachromosomal translocation (fusion) involving chromosome 10 (Fig. 4C), which was the inversion of the FGFR2 containing protein kinase domain.

4. Discussion

In this study, we report 7 cases of MVNT, which are unique epilepsy-associated neuronal tumors and most commonly occur in adults. We reviewed previous articles on MVNTs (Table 3) [1-8,11-19]. Although this tumor commonly develops in adults (median age of adult cases, 43 years; range, 21−71 years), to date, 6 pediatric and adolescent cases, including our 1 pediatric case (median age of child cases, 11.5 years; range, 6-19 years) have been reported [4,5]. There was a slight female predominance (male-to-female ratio, 1:1.15). All tumors developed in the cerebrum, and almost 80% of them occurred in the temporal (46%) and frontal lobes (34%).

Previous studies indicated that MVNT is an indolent tumor or lesion, consistent with WHO grade I. The 62 previously reported cases showed no recurrence of tumors after resection [1-8,11-19]. One of our cases underwent a second operation because of sustained intractable seizures resulting from a 0.5-cm-sized residual tumor; however, there were no recurrent cases.

MRI findings were unique in our cases; multilobulated masses with hyperintense signals on T2 and FLAIR and hypointense or isointense signals on T1 with no enhancement. Our cases showed

Table 4 Reported found genetic abnormalities in MVNTs

No	Sex/age (y)/presentation	Genetic variation	Article
1	M/35/episodic confusion (14 mo)	*MAP2K1* p.T55_V60delinsT	Pekmezci et al [5] (originally the case of Huse et al [1])
2	M/54/seizures (>40 y)	*MAP2K1* p.Q56P	Huse et al [1]
3	F/63 numbness and tingling (1 y)	*MAP2K1* p.Q56P	Pekmezci et al [5] (originally the case of Huse et al [1])
4	M/43/headaches	*MAP2K1* p.Q56_G61delinsL	Pekmezci et al [5]
5	F/19/seizure	*MAP2K1* p.K57_E62delinsK	Pekmezci et al [5]
6	F/54/headache	*BRAF* p.L597R	Pekmezci et al [5]
7	F/11/seizures	*BRAF* p.G469S	Pekmezci et al [5]
8	M/12/seizures	*FGFR-INA* gene fusion	Pekmezci et al [5]
9	F/59/seizure (20 y)	*DEPDC5*, *SMO*, *TP53*, *CIC*	Thom et al [4] (originally the case of Ratilal et al [3])
10	F/32/seizure	*SUFU*, *DEPDC5*, *SMO*, *TP53*, *NPRL3*, *PIK3CA*	Thom et al [4]
11	F/27/seizure (17 y)	*DEPDC5*, *SMO*, *TP53*, *NPRL3*, *CIC*, *PIK3CA*	Thom et al [4]
12	F/67/seizure (2 y)	*DEPDC5*, *SMO*, *TP53*, *NPRL3*, *PIK3CA*	Thom et al [4]
13	F/48/seizure (1 y)	*DEPDC5*, *SMO*, *TP53*, *NPRL3*, *CIC*, *PIK3CA*	Thom et al [4]
14	M/54/seizure (33 y)	*EZH2*, *DEPDC5*, *SMO*, *TP53*, *CIC*, *PIK3CA*	Thom et al [4]
15	F/41/seizure	*DEPDC5*, *SMO*, *TP53*, *NPRL3*, *CIC*, *PIK3CA*	Thom et al [4]
16	M/55/seizure	*DEPDC5*, *SMO*, *TP53*, *CIC*, *PIK3CA*	Thom et al [4]

somewhat ill-defined circumscription on MRI. The clinical findings in our cases are summarized in Tables 1 and 2, and findings from previous reports are described in Table 3.

Two of our cases revealed definite nuclear atypia, such as enlargement and multiple nuclei (Fig. 2), which could be present in MVNT. However, this might be a degenerative nuclear atypia introduced by the long-standing and slow-growing nature of these tumors. There were no Rosenthal fibers, eosinophilic granular bodies, or perivascular lymphocytic infiltration. Microcalcification was not found in the previously reported MVNTs as well. Moreover, there were no oligodendroglia-like cells. Therefore, MVNT is different from the polymorphous low-grade neuroepithelial tumor of the young or dysembryoplastic neuroepithelial tumor or GG.

In our cases, the vacuolated tumor cells appeared like "immature-looking" neuronal cells, which were supported by positive results for synaptophysin and MAP2 and robust expression of α-INA and Olig2, but negative results for NeuN. GFAP was positive only in the background of the tumor cells, but tumor cells were completely negative for GFAP. α-INA is an intermediate neurofilament seen in early developing neurons [12]. α-INA was diffusely and intensely positive in 5 cases but partly positive in 2 cases. Because of Olig2 positivity in vacuolated tumor cells, these cells might have originated from Olig2-positive neuroglial progenitors, with developmentally arrested or partial or aberrant maturation to a neuronal phenotype. CD34 is a stem cell factor and is known to be positive in ganglion cell tumors, at least focally as a ramifying or dendritic cell pattern. In our series, CD34 and nestin were all negative in tumor cells. Above-described immunophenotypic features distinguish MVNT from classic neuronal or mixed glioneuronal tumors of the central nervous system.

In the current study, electron microscopic study also revealed the neuronal nature of vacuolated tumor cells: this vacuolation might be produced by pericellular empty space rather than by cytoplasmic vacuolation. The cytoplasm of these cells frequently had at least several myelin-like autophagolysosomes or enigma body–like conglomerated lipofuscin bodies.

Pekmezci et al [5] reported that these tumors are mixtures of neoplastic neuronal cells and small glial cells, and both cell types are positive for phospho-ERK. Moreover, Thom et al [4] reported that the expression patterns of GFAPδ, pS6, PDGFRβ, PAX6, nestin, and OLIG2 suggest a mixed cellular composition in MVNT. However, most authors have described MVNT as a purely neuronal tumor.

WES was performed in 4 of our cases, but there were no meaningful molecular alterations related to the development of MVNT, except for the *FGFR2-ZMYND11* intrachromosomal translocation involving chromosome 10 in 1 case. The biologic characteristics of MVNT including a slow-growing nature, very low proliferation index, absence of apparent genetic alterations, and coexistence with cortical dysplasia in some cases suggested that MVNTs may be hamartomas rather than true neoplastic lesions. However, a single-point mutation involving *MAP2K1* (*MEK1*) in 1 case of the series of Huse et al [1] suggested the possibility that neoplastic processes could be involved. In addition, Pekmezci et al [5] demonstrated mutations in the *BRAF* gene (p.L597R and p.G469S) and exon 2 of *MAP2K1* (p.Q56P), and 1 case with an *FGFR2-INA* in-frame gene fusion. Therefore, Pekmezci et al suggested that alteration of the MAPK signaling pathway is strongly associated with MVNTs. However, our 4 cases revealed neither *BRAF* nor *MAP2K1* gene mutations. Previously found genetic abnormalities of MVNTs are summarized in Table 4.

Among the 4 cases in this study for which WES was performed, only 1 case revealed an intrachromosomal gene fusion, *FGFR2-ZMYND11*, on chromosome 10 (Fig. 4). With Integrative Genomics Viewer, we found that an inversion had occurred. However, there were no other meaningful mutations or chromosomal copy number aberrations. To date, we could not find reports of *FGFR2-ZMYND11* fusion associated with cancer or glioma in the available literature. However, *FGFR2-PPHLN* fusion was reported in cholangiocarcinoma [20], and *ZMYND11*/*MBTD1* gene fusion was found to be associated with acute myeloid leukemia [21,22].

FGFR protein is composed of 3 immunoglobulin-like domains and 1 cytoplasmic tyrosine kinase domain. With the help of freely accessible protein sequence database (https://www.uniprot.org/uniprot/P21802#family_and_domains), reference sequence database (RefSeq [FGFR2, transcript variant 1, Accession ID: NM_000141.4]), and human genome browser (hg19), we ascertained that the suspected breakpoint of the *FGFR2* gene does not involve any major domains but is located downstream of the protein kinase domain with an interval of less than 20 bp.

The extracellular portion of the FGFR protein is known to interact with fibroblast growth factors and ultimately influences mitogenesis and differentiation. This particular family member is a high-affinity receptor for acidic, basic, and/or keratinocyte growth factors, depending on the isoform involved. Multiple alternatively spliced transcript variants encoding different isoforms have been noted for this gene. *FGFR* fusions form as a result of various mechanisms—predominantly deletions of *FGFR1*, translocations involving *FGFR2*, and tandem duplications of *FGFR3* [23].

5. Conclusion

We reported 7 cases of MVNT, which were distinct epileptogenic neuronal tumors of the adult cerebrum. The vacuolated tumor cells were most likely immature neuronal cells. So far, they are described as benign, WHO grade I. We found *FGFR2-ZMYND11* fusion in 1 case. Additional genomic studies in more cases are required to verify the molecular and biologic nature of this tumor type and to identify potential therapeutic targets.

Supplementary data

Supplementary data to this article can be found online at https://doi.org/10.1016/j.humpath.2018.11.028.

References

[1] Huse JT, Edgar M, Halliday J, Mikolaenko I, Lavi E, Rosenblum MK. Multinodular and vacuolating neuronal tumors of the cerebrum: 10 cases of a distinctive seizure-associated lesion. Brain Pathol 2013;23:515-24. https://doi.org/10.1111/bpa.12035.

[2] Yamaguchi M, Komori T, Nakata Y, Yagishita A, Morino M, Isozaki E. Multinodular and vacuolating neuronal tumor affecting amygdala and hippocampus: a quasi-tumor? Pathol Int 2016;66:34-41. https://doi.org/10.1111/pin.12366.

[3] Ratilal B, McEvoy A, Sisodiya S, Thom M, Toma A. Diffuse cerebral gangliocytoma in an adult with late-onset refractory epilepsy. Neuropathol Appl Neurobiol 2007;33:706-9. https://doi.org/10.1111/j.1365-2990.2007.00861.x.

[4] Thom M, Liu J, Bongaarts A, Reinten RJ, Paradiso B, Jäger HR, et al. Multinodular and vacuolating neuronal tumors in epilepsy: dysplasia or neoplasia? Brain Pathol 2018;28:155-71. https://doi.org/10.1111/bpa.12555.

[5] Pekmezci M, Stevers M, Phillips JJ, Van Ziffle J, Bastian BC, Tsankova NM, et al. Multinodular and vacuolating neuronal tumor of the cerebrum is a clonal neoplasm defined by genetic alterations that activate the MAP kinase signaling pathway. Acta Neuropathol 2018;135:485-8. https://doi.org/10.1007/s00401-018-1820-4.

[6] Bodi I, Curran O, Selway R, Elwes R, Burrone J, Laxton R, et al. Two cases of multinodular and vacuolating neuronal tumour. Acta Neuropathol Commun 2014;2:7. https://doi.org/10.1186/2051-5960-2-7.

[7] Fukushima S, Yoshida A, Narita Y, Arita H, Ohno M, Miyakita Y, et al. Multinodular and vacuolating neuronal tumor of the cerebrum. Brain Tumor Pathol 2015;32:131-6. https://doi.org/10.1007/s10014-014-0198-9.

[8] Nagaishi M, Yokoo H, Nobusawa S, Fujii Y, Sugiura Y, Suzuki R, et al. Localized overexpression of alpha-internexin within nodules in multinodular and vacuolating neuronal tumors. Neuropathology 2015;35:561-8. https://doi.org/10.1111/neup.12217.

[9] Koh J, Cho H, Kim H, Kim SI, Yun S, Park C-K, et al. IDH2 mutation in gliomas including novel mutation. Neuropathology 2015;35:236-44. https://doi.org/10.1111/neup.12187.

[10] Myung JK, Cho H, Park C-K, Kim S-K, Lee S-H, Park S-H. Analysis of the BRAF(V600E) mutation in central nervous system tumors. Transl Oncol 2012;5:430-6. https://doi.org/10.1593/tlo.12328.

[11] Gökçe E. Magnetic resonance imaging findings of two cases with multinodular and vacuolating neuronal tumor. Acta Neurol Belg 2017:1-5. https://doi.org/10.1007/s13760-017-0872-x.

[12] Lobo R, Srinivasan A. Case of the season: multinodular and vacuolating neuronal tumor. Semin Roentgenol 2018;53:3-5. https://doi.org/10.1053/j.ro.2017.11.001.

[13] Shitara S, Tokime T, Akiyama Y. Multinodular and vacuolating neuronal tumor: a case report and literature review. Surg Neurol Int 2018;9:63. https://doi.org/10.4103/sni.sni_348_17.

[14] Kapucu I, Jhaveri MD, Kocak M, Kontzialis M. Multinodular and vacuolating neuronal tumor of the cerebrum: a benign nonaggressive cerebral lesion. Eur Neurol 2018;79:74-5. https://doi.org/10.1159/000485670.

[15] Nunes RH, Hsu CC, Da Rocha AJ, Do Amaral LLF, Godoy LFS, Watkins TW, et al. Multinodular and vacuolating neuronal tumor of the cerebrum: a new "leave me alone" lesion with a characteristic imaging pattern. Am J Neuroradiol 2017;38:1899-904. https://doi.org/10.3174/ajnr.A5281.

[16] Gonzalez-Quarante LH, Ruiz-Juretschke F, Sola VE, Gil de Sagredo del Corral OL, Agarwal V, Garcia-Leal R. Multinodular and vacuolating neuronal tumor of the cerebrum. A rare entity. New case and review of the literature. Neurocirugia 2018;29:44-55. https://doi.org/10.1016/j.neucir.2017.08.003.

[17] Cathcart SJ, Klug JR, Helvey JT, White ML, Gard AP, McComb RD. Multinodular and vacuolating neuronal tumor. Am J Surg Pathol 2017;41:1005-10. https://doi.org/10.1097/PAS.0000000000000868.

[18] Alsufayan R, Alcaide-Leon P, de Tilly LN, Mandell DM, Krings T. Natural history of lesions with the MR imaging appearance of multinodular and vacuolating neuronal tumor. Neuroradiology 2017;59:873-83. https://doi.org/10.1007/s00234-017-1884-1.

[19] Badat N, Savatovsky J, Charbonneau F, Collin A, Lecler A. Multinodular vacuolating and neuronal tumor of the cerebrum. Neurology 2017;89:304-5.

[20] Sia D, Losic B, Moeini A, Cabellos L, Hao K, Revill K, et al. Massive parallel sequencing uncovers actionable FGFR2-PPHLN1 fusion and ARAF mutations in intrahepatic cholangiocarcinoma. Nat Commun 2015;6:6087. https://doi.org/10.1038/ncomms7087.

[21] de Rooij JDE, van den Heuvel-Eibrink MM, Kollen WJW, Sonneveld E, Kaspers GJL, Beverloo HB, et al. Recurrent translocation t(10;17)(p15;q21) in minimally differentiated acute myeloid leukemia results in ZMYND11/MBTD1 fusion. Genes Chromosomes Cancer 2016;55:237-41. https://doi.org/10.1002/gcc.22326.

[22] De Braekeleer E, Auffret R, Douet-Guilbert N, Basinko A, Le Bris M-J, Morel F, et al. Recurrent translocation (10;17)(p15;q21) in acute poorly differentiated myeloid leukemia likely results in ZMYND11-MBTD1 fusion. Leuk Lymphoma 2014;55:1189-90. https://doi.org/10.3109/10428194.2013.820292.

[23] Parker BC, Engels M, Annala M, Zhang W. Emergence of FGFR family gene fusions as therapeutic targets in a wide spectrum of solid tumours. J Pathol 2014;232:4-15.